Applied Catalysis B: Environmental 160–161 (2014) 22–34

Contents lists available at ScienceDirect

Applied Catalysis B: Environmental

journal homepage: www.elsevier.com/locate/apcatb

Structure-reactivity relationship in catalytic hydrogenation of heterocyclic compounds over ruthenium black-Part A: Effect of substitution of pyrrole ring and side chain in *N*-heterocycles

Katarzyna Morawa Eblagon, S.C.Edman Tsang*

Wolfson Catalysis Centre, Department of Chemistry, Inorganic Chemistry Laboratory, University of Oxford, South Parks Road, Oxford OX1 3QR, UK

ARTICLE INFO

Article history:
Received 14 November 2013
Received in revised form 14 April 2014
Accepted 25 April 2014
Available online 4 May 2014

Keywords:
Hydrogen storage
Carbazole
Thermodynamic
Kinetic
Ruthenium

ABSTRACT

The catalytic hydrogenations of carbazole, 9-carbazole-9*H*-ethanol and acridine over Ru black were studied and compared with the results obtained from 9-ethylcarbazole with the aim to elucidate the influence of the molecules structures on their ability to store hydrogen. The reactions were modelled with the rate constants derived for each of the elementary reactions observed. The specific catalytic activity and selectivity were found to be strongly dependent on variation in the structure of substrate due to both thermodynamic and kinetic reasons. The hydrogenation activity was found to increase in order: acridine > 9-*H*-carbazole-9*H*-ethanol > carbazole > 9-ethylcarbazole. The hydrogenation pathway of the molecule consisting of six-membered ring (acridine) was found to be more complex than that of a corresponding five-membered ring structure. The type of intermediates also appeared to depend on the basicity and steric environment of the nitrogen heteroatom, which influenced the geometry of the adsorption on the ruthenium surface. It is believed that this work can provide some general guidelines for the design of superior liquid organic carriers (LOCs).

1. Introduction

The use of aromatic-aliphatic compounds known as liquid organic carriers (LOCs) as a possible mean to carry hydrogen chemically for the mobile applications of H_2 powered polymer membrane fuel cells (PEMFC) is currently under intense research [1–4]. Systems such as toluene–methylcyclohexane [5] or naphthalene–decalin [6] are capable of taking up a substantial amount of hydrogen in a cyclic manner [7]. There is a vast amount of information available in the literature concerning mainly the influence of different parameters on the dehydrogenation step (hydrogen release step) of the LOC [2,5,8–10]. For example, Schwarz et al. studied the dehydrogenation of benzimidazoles for applications as hydrogen storage media and found some of the dehydrogenation reactions to be more exergonic than others, depending on the structure of the compounds [8].

On the other hand, there is still a very limited amount of published work dealing with the influence of structure on ability to hydrogenate (to store hydrogen) over metal catalysts. For example, Sakanishi et al. [11] examined the reactivity of a wide variety of polyaromatic compounds in hydrogenation over supported Pt, Pd, Ru and Rh catalysts. This work was followed by Sotoodeh et al. who studied the hydrogenation of carbazole and 9-ethylcarbazole over supported commercial Ru catalyst [12]. However, the recyclability of liquid organic carrier is crucial with respects to economic and energy aspects. As a result, in order to design new LOCs with improved kinetics and thermodynamics of reversible hydrogenation/dehydrogenation process, it is of great importance to understand the relationship between structure and performance. From the point of view of application in reversible hydrogen storage, complete hydrogenation of a chemical carrier (thermodynamically favorable under reaction conditions) with fast kinetics into desired product without competition from any side reactions is desirable. In addition, the high stereoselectivity toward cis-isomers of the fully saturated product would be more preferable over the thermodynamically favored trans-stereoisomers due to the former being easier to dehydrogenate on catalytic surface with lesser steric hindrance [13]. Any side reactions such as hydrogenolysis, cracking or ring opening and hydrodenitrogenation would not only reduce the overall hydrogen carrying capacity of the system but may also require an expensive purification procedure. Nevertheless, hydrogenation of aromatics over heterogeneous catalysts normally takes place via several consecutive steps with competitive side reactions [11].

* Corresponding author.
E-mail address: edman.tsang@chem.ox.ac.uk (S.C.Edman Tsang).

http://dx.doi.org/10.1016/j.apcatb.2014.04.044
0926-3373/

In our previous works [14–16] a reversible hydrogen storage system based on 9-ethylcarbazole as a prototype of LOC was extensively studied over various supported and unsupported noble metal catalysts. It was found that the hydrogenation of 9-ethylcarbazole over commercial ruthenium black catalyst resulted in the formation of a kinetically stable intermediate; 9-ethyl-octahydrocarbazole (addition of 8 hydrogen atoms, encoded as Pl 8[H]), which led to a poor selectivity of the reaction toward the fully loaded products [14]. The formation of such stable intermediate products should be avoided in LOC systems. Thus, in the light of our previous findings and with regards to hydrogen storage application, the focus of the present work is to investigate the influence of the structure of heterocyclic compound on the intermediates and products during its hydrogenation (fuel recovery) over a ruthenium black commercial catalyst. Thus, the effects of structural features on the presence of any side reactions, poisoning of the surface active sites of the catalyst and kinetics of hydrogen uptake are of a particular interest here. Finally, the effect of structural aspects of LOC that can improve recyclability will be discussed in order to establish general guidelines for the rational design of new LOCs with improved kinetics and thermodynamics of reversible chemical hydrogen storage for mobile applications.

2. Experimental

2.1. Materials

9-Ethylcarbazole (97%), 1,4-dioxane (ACS reagent ≥99%), 1,2,3,4-tetrahydrocarbazole ≥99%, carbazole (≥95%), 9*H*-carbazole-9-ethanol (95%), 1,4-dioxane (ACS reagent 99%) and Ru black catalyst were purchased from Sigma-Aldrich. Hydrogen gas (99.9%) was supplied by Air-Products. The structural variations of heterocyclic compounds studied in this present work are gathered in Table 1. The Ru black catalyst was chosen in the present study due to the fact that a significant quantity of a very stable Pl 8[H] intermediate was formed over this catalyst during the hydrogenation of 9-ethylcarbazole [14]. Thus, it would be of interest to determine if similar intermediates can be formed over the same catalyst during hydrogenation of other heterocyclic compounds with similar structures. In addition, the absence of the support in this catalyst eliminates the complex metal-support interactions that affect the hydrogenation steps. It should be noted that electronic states hence catalytic properties of metal nanoparticles can be changed by their degree of dispersion, type of support used or possible electron transfer at the catalyst-support interface [17,18]. The chosen molecules shown in Table 1, all contain N heteroatom and only differ from each other in one structural aspect. The investigated structural factors include: difference in side chain length and substitution of a pyrrole ring (five-membered ring) with pyridinic ring (six-membered ring).

2.2. Catalyst characterization

The characterization of physical and chemical properties of a catalyst is essential to gain understanding of interactions between metal surface, substrate and intermediates of the reaction. Ru black commercial catalyst from Sigma-Aldrich was characterized in our previous work [14,15] using various methods such as CO-pulse chemisorption, high resolution transmission electron microscopy (HRTEM) and CO adsorption coupled with diffusion reflectance infrared Fourier transform (CO-DRIFT). In addition, the composition and morphology of Ru black catalyst before and after the hydrogenation reactions were obtained using X-ray diffraction analysis (XRD). In a typical XRD experiment, about 0.15 g of powder Ru catalyst sample was used. The sample was grinded using paste and mortar to obtain a fine powder of less than 200-mesh size. Subsequently, the catalyst powder was placed on a glass slide and smothered with a glass slid to ensure a highly leveled sample. The prepared sample was loaded into a Philips DIFF 3, X-ray diffractometer with a Cu-anode source operating at 40 kV and 30 mA generating Cu $K\alpha$ X-ray radiation at wavelengths Cu $K\alpha_1$ = 1.5406 Å and Cu $K\alpha_2$ = 1.54439 Å. The data was collected at 2θ from 5° to 70° angles, with a step size of 0.02°, step speed of 0.5 min^{-1} and at 1.25 s per step. The obtained X-ray diffraction patterns were compared to those of a standard database and the phases were assigned using X'Pert software.

The surface composition of the catalyst was probed using X-ray photoelectron spectroscopy (XPS). In a typical XPS measurement, 0.05 g of solid sample was grinded in a mortar and subsequently sprinkled on a copper plate with silver paste. The XPS spectra were measured with a Leybold LH 10 spectrometer equipped with a single-channel detector, employing Mg $K\alpha$ radiation (1253.6 eV, anode operated at 10 kV × 23 mA). The Ru (3d) with C (1s) superimposed spectra was recorded with the analyzer in constant pass-energy mode (pass energy at 50 eV). The XPS peaks were fitted using curve-fitting XPSPEAK41 software, by choosing the appropriate background and peak shapes. Careful deconvolution was performed consisting of the calibration of peak positions against the C 1s line and application of a Shirley background. All of the XPS spectra were deconvoluted into symmetric Gaussian 80%-Lorentzian peaks following the guidelines in the literature [19].

2.3. Hydrogenation procedures

A series of polycyclic heteroaromatic compounds with their structures shown in Table 1 were hydrogenated in the liquid phase in a stainless steel batch-type Parr autoclave reactor. In a typical experiment, 3 g of substrate (Table 1) was dissolved in 100 mL of 1,4-dioxane solvent with added 0.15 g of Ru black catalyst. The batch reactor was then sealed, flushed with hydrogen and heated to 130 °C. When the desired temperature was reached, 70 bar of pure hydrogen was charged into the reactor and the reaction time was started. During the reaction, a magnetic stirrer with a stirring speed of 600 rpm was used. After the required reaction time, the autoclave was cooled down to room temperature, the pressure was released and the reaction mixture was analyzed. The hydrogenation reactions of all of the heterocyclic compounds were studied under the same testing conditions which were previously used for the hydrogenation of 9-ethylcarbazole [14]. In order to obtain time versus concentration profiles, small aliquots of the reaction solution were removed periodically from the reactor for analysis. Control experiments were carried out, in which the hydrogenation reaction of 9-ethylcarbazole over the Ru black catalyst was tested four times under the same reaction conditions and the results showed a variation within 5% in the values of conversion and selectivity.

2.4. Analysis of the hydrogenation products

The intermediates and products of all the hydrogenation reactions over Ru black catalyst were detected and separated using a GC–MS system (Agilent 6890-5975E GC–MS) equipped with a non-polar capillary column (Agilent 19091s-433), an auto-sampler and MSD-Triple Axis Detector HED-EM mass detector, using He as a carrier gas. The structures of the final products and intermediates of the reactions were assigned based on their electron impact mass spectra that corresponded to the database of the GC–MS system. Before analysis, individual calibration curves were also prepared for each of the reactions analyzed, running at least five different concentrations of the starting material with the designed time-temperature program. The time-temperature program was varied

Table 1
Structures and properties of heterocyclic compounds considered for chemical hydrogen storage materials in the present work.

Molecule name	Molecular structure	Molar mass (g/mol)	Theoretical maximum hydrogen uptake (%)
9-Ethylcarbazole	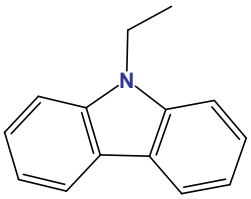	195.26	5.8
Carbazole	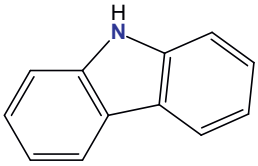	167.2	6.7
Carbazole-9-ethanol	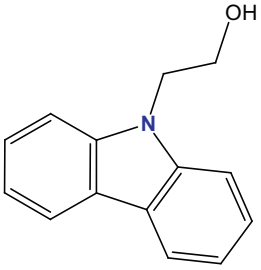	211.3	5.4
Acridine	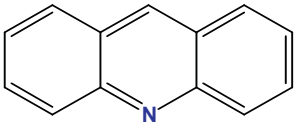	179.2	7.2

according to the structure of the molecule of interest. The total reaction time was 7 h.

The selectivity of the reactions was calculated according to the equation:

$$\text{selectivity}\,(\%) = \frac{\text{amount of selected product(moles)}}{\text{sum of all the products(moles)}}100\% \quad (2.4.1)$$

2.5. Modeling of the reactions pathway

Based on the obtained profiles of concentration versus time, a preliminary kinetic model was used to derive a number of rate constants for each of the hydrogenation reaction studied. Similar procedure was developed and applied previously in case of the hydrogenation of 9-ethylcarbazole over Ru catalysts [14,15]. In this model, a series of differential equations were first derived for each of the intermediate compounds observed in the solution. These equations can be solved by fitting the concentration-time profiles of the species with a kinetic model using the 4th and 5th order Runge–Kutta formulas [20] with the following boundary conditions imposed. For example, at the starting point (time = 0 [s]) the concentration of the substrate was 100% ([P_0] = 100 (mol%)) and the concentrations of all other species were zero. The first rate constant, k_0, was determined by a regression analysis of the P_0 concentration-time profile (derived from the conversion) against a simple first order integrated rate law as described earlier [15]. Additionally, k_0 was the overall first order decomposition rate constant of the starting material, and was equal to the summation of all the other rate constants of all intermediate reactions. The other rate constants were derived using a Nelder–Mead method (simplex method) for systematic comparison [21]. The mismatch between experimental and modeled values was calculated minimizing the root mean square between the model and the experimental data (RMS) [22]. The calculations were continued until the convergence criteria were satisfied and the mismatch was not greater than the pre-set value. In case when a local minimum was found by the software, the k values were modified accordingly to allow better optimization of the fit. Thus, a reaction model can then be developed by taking into account the structures of the intermediates obtained experimentally and identified using GC–MS and the changes of their concentrations with time. The first working model is subsequently refined by removing the unimportant reaction steps that showed calculated k values $\leq$0 or approaching 0. The required calculations were performed using MathLab (version 7.5). The typical concentration profiles of substrate, intermediates and products are presented in the main text of the manuscript. Selected enlarged parts of the corresponding concentration versus time plots are presented in the Supplementary material in Figs. 1s–3s. In these enlarged figures only the intermediates and products which appear at lower concentrations are displayed, which allows to present more precisely the relevance of the kinetic models proposed in the present work.

2.6. DFT calculations of enthalpies

In order to gauge the thermodynamic stability of some intermediates out of a number of possible structures, the energies (total enthalpies) were calculated. These quantum mechanics calculations were performed using Gaussian 03 software [23] and the identified possible stable intermediates were compared with the ones observed during the experiments. A similar procedure was already applied in our previous work concerning hydrogenation

Table 2
Physical properties of Ru black commercial catalyst [14].

Catalyst	Primary particle size TEM (nm)	Dispersion (%)	Metal area (m^2/g)	BET surface area (m^2/g)	Average pore diameter (nm)
Ru black	6.3 (strongly aggregated)	1.01	4.78	22.2	24.4

of 9-ethylcarbazole [14,24]. In short, all the calculations were performed with a 6-311 + G (3df, 2p) basis set, which provided the electronic energy for the geometric optimized molecules and a B3LYP hybrid functional method for electron correlation [25]. The same basis set was also used for the estimation of vibrational energies. Thus, the thermodynamic parameters of products and intermediates involving transitional, rotational and translational modes were taken into account. Subsequently, the calculated total enthalpy (the sum of electronic energies found from geometric calculations, and thermal, translational and vibrational energies) was compared to the sum of enthalpies for the starting material together with the total enthalpy of the moles of hydrogen added to create the defined intermediate product, as previously described [14]. In order to introduce the thermal effects, the total enthalpies for all of the hydrogenation reactions studied were calculated including thermal contributions to the free energies of the molecule at 403 K, which was the reaction temperature used throughout all of the hydrogenation experiments. All of the calculations were done in a gas phase approximation. Therefore, it should be highlighted that this approach brings about some limitations and as such, the presented results should be treated as basic illustration of general trends of stability of the reaction products and intermediates, not as absolute values. One of the most important approximations of this approach is that all of the equations used in computing thermochemistry data assume non-interacting particles and therefore apply solely to the ideal gas. As a result, the error of the resulting enthalpy depends on the degree in which the studied system differs from the ideal gas [23,25]. In addition, the minor error can be introduced by the fact that in order to calculate the electronic contributions higher excited states were assumed to be not accessible. Moreover, it should be underlined that the properties of the molecules as well as their interaction between each other and their transition states can differ considerably between gas phase and the solution (e.g. cohesive energy of the molecules in the solvent). Additionally, it is clear that the enthalpy of the compounds depends on the solvent medium. However, these DFT calculations do not take into account the solvation effects on the reactants, products and intermediates, nor the differences in solvation energy of transition states. Furthermore, the presence of the catalyst is also not considered here. However, all of these factors govern the adsorption geometry of the substrates and products and thus can alter the reaction pathway. Overall, our DFT calculations enable the structural comparison between substrates and intermediates in terms of their thermodynamic stability to be relatively easily made without taking into account the complex entropic factors, which would require further expensive computing time. In addition, the difference in ΔS between each of the molecular conformations studied here is not expected to be large at the reaction temperature considered.

3. Results and discussion

3.1. Catalyst characterization

It is of interest to know whether the production of the stable intermediates or the occurrence of any side reactions is influenced by the structure of the substrate itself. Therefore, a well characterized commercial Ru black catalyst was used for all of the hydrogenations studied and the reactions were performed under identical conditions of hydrogen pressure and temperature in order to evaluate solely the interaction between the substrate and the active sites of the Ru metal catalyst. The physical and chemical properties of the Ru black obtained in our previous work [14] are gathered in Table 2. As it can be seen in this table, the Ru black commercial catalyst has low metal dispersion, thus the number of active sites available for the reaction is limited. However, based on our previous theoretical findings concerning 9-ethylcarbazole [14], it is evident that there was no site competition between H_2 and substrates on the surface of Ru black catalyst. However, the low number of the active sites in this catalyst is responsible for slow reaction rates as compared to other Ru based catalysts. The greater number of terrace sites over step, edge or adatom sites on Ru black (the catalyst was exposed to high temperatures during its manufacture process) can exert a strong influence on the adsorption geometries of bulky substrates. HRTEM images (shown in Fig. 1) of Ru black indeed suggest a high proportion of faceted (flat) surfaces which were found to provide less efficient sites in the hydrogenation of 9-ethylcarbazole than highly unsaturated sites due to the presence of steric hindrance [14].

The HRTEM images of the Ru black catalyst shown in Fig. 1 depict some strongly sintered Ru nanoparticles that form large, irregularly shaped aggregates. In addition, some large faceted Ru nanoparticles are decorated with smaller particles. This morphology of the commercial Ru black sample was produced by the high temperature

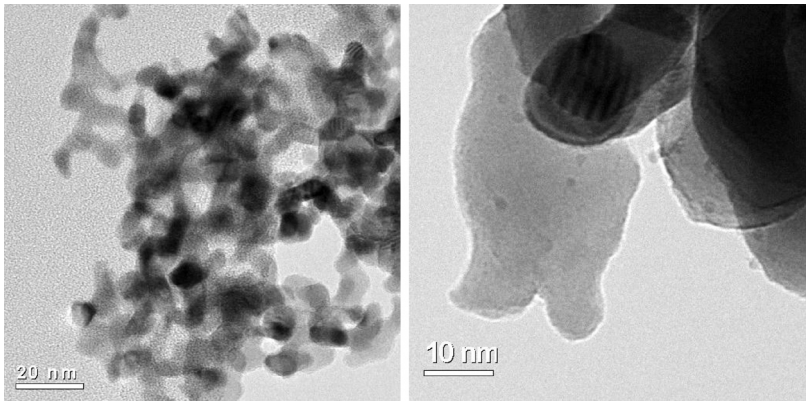

Fig. 1. HRTEM images of Ru black commercial catalyst.

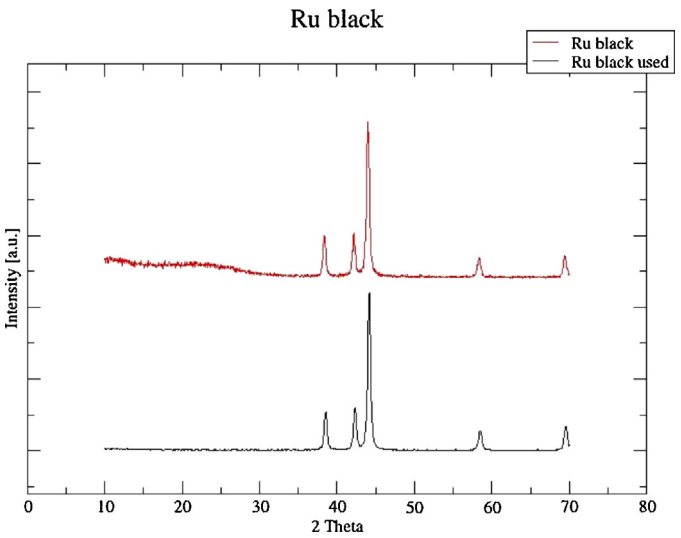

Fig. 2. XRD pattern of Ru black catalyst before and after 20 h of carbazole hydrogenation.

heat treatment. As the result, such unsupported particles had sintered to minimize their excess of surface energy and therefore significantly lower dispersion of this catalyst can be expected in comparison with the corresponding supported catalytic systems having similar average particle size.

The corresponding XRD patterns of the Ru black catalyst before and after hydrogenation of carbazole (Table 1) are shown in Fig. 2. The sharp distinct diffraction peaks at 38.1°, 42.6°, 44.7° and 58.4° are consistent with the low indexed (1 0 0), (0 0 2), (1 0 1), and (1 0 2) planes of bulk hexagonal ruthenium (ICDD-JCPDS Card no. 06-0663). The obtained sharp diffraction lines suggest a highly ordered structure of large ruthenium metal crystallites. This finding agrees well with the results from HRTEM studies. In addition, the XRD analysis confirmed that the catalyst contained most ruthenium atoms in zerovalent state. It should be noted that the diffraction patterns of the spent Ru black catalyst remained almost unchanged as compared to that of a fresh catalyst, indicating significant stability of this catalyst under the reaction conditions despite the absence of support. However, detailed inspection of Fig. 2 reveals a slight increase in particle size after reaction, as reflected by sharper diffraction peaks. In addition, no carbon residues were noted on the XRD spectra of the used catalyst, proving that there was no significant coke formation under the reaction conditions. Similar results were observed in cases of other reactants.

In Table 2 a large discrepancy can be noted between the metal surface measured by CO chemisorption and the N_2 BET surface area of this pure metal catalyst. However this could be easily explained by the fact that in a classical measurement of the surface area of a noble metal nanoparticles by CO chemisorption the knowledge/assumption of the M–CO stoichiometry is required. Thus, for a small particle the stoichiometry of CO/M = 1 (our equipment was set as 1) is commonly used. However, for the large faceted particle, a bridging mode of absorption of CO species is expected to be dominant over linear mode. As a result, the actual metal surface area could be underestimated by the CO chemisorption. In addition, we have observed a presence of some carbonaceous species on the surface of the ruthenium black catalyst in the XPS experiment (see the next paragraph), which can significantly block the CO gas accessibility to the active sites and thus decrease the extent of chemisorption. Moreover, these carbon species could also alter the mode of adsorption of CO on the surface of the catalyst.

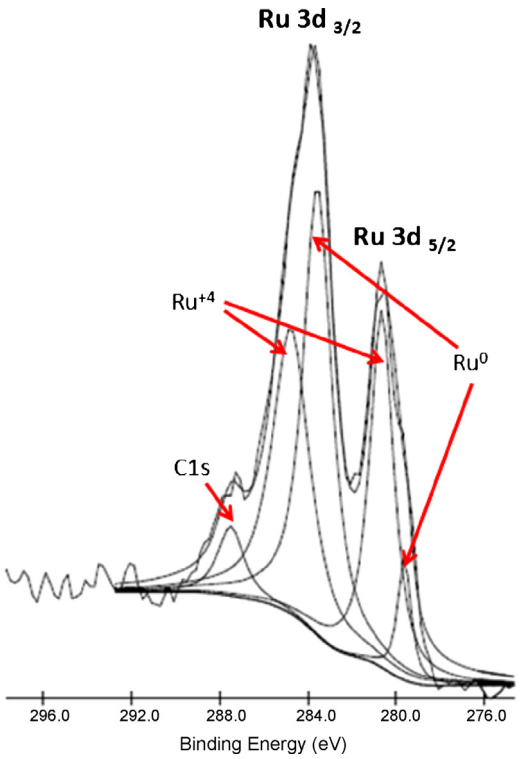

Fig. 3. The Ru $3d_{3/2}$ and Ru $3d_{5/2}$ XPS region of ruthenium black catalyst; the fitting line is shown as a weaker solid line.

The XPS measurements shown in Fig. 3 displayed the existence of two different ruthenium species in the Ru black catalyst. Peaks at 279.6 eV and 284.8 eV can be attributed to the two spin orbital coupling peaks of ruthenium in metallic state (Ru^0) [19,26,27]. The binding energy of Ru^0 $3d_{5/2}$ obtained for ruthenium black in our work (279.6 eV) is in a good agreement with the value of 280.2 eV reported for ruthenium black catalyst by Larichev [27]. On the other hand, the two other spin orbital coupled peaks found at 280.7 eV and 285.5 eV were assigned to oxidized ruthenium species (RuO_2) [28–30]. During the transfer of a sample to the XPS equipment, the presence of oxidized ruthenium on the surface of the catalysts cannot be avoided, due to the fact that ruthenium metal can be oxidized very easily in air even at room temperature. However, the quantitative analysis of Ru^{4+} and Ru^0 cannot be conducted because of severe overlapping of the peaks which does not allow reliable integration of the peak areas. The peak at 287.5 eV was assigned to carbonaceous species associated with hydrogen or/oxygen [31] or C=O structures [32]. These surface compounds probably originated from the commercial procedure of the catalysts manufacture.

3.2. *Influence of the structure of LOC on its ability to dehydrogenate*

The application of the selected materials for hydrogen storage is dependent on their ability to reversibly hydrogenate and dehydrogenate with high selectivity under reasonable reaction conditions. Therefore, the kinetics of dehydrogenation of these materials should be considered and balanced with the kinetics of the reversed reaction in order to select the most suitable LOC. The hydrogen storage based on heterocyclic compounds was first introduced by Air Products in the series of patents [33,34], where some general trends for optimizing the structure of LOC were established. It was found that incorporation of N into a six-membered ring favors thermodynamics of hydrogen release by lowering the standard enthalpy of hydrogenation of the compound. This can be

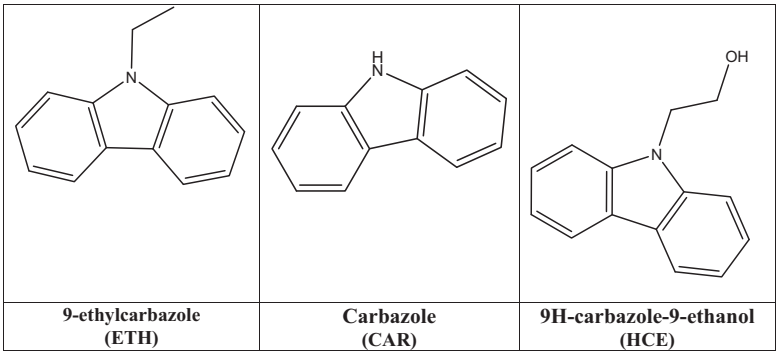

Fig. 4. Chemical structures of heterocyclic polyaromatic compounds with different length and chemical composition of a side chain attached to nitrogen heteroatom.

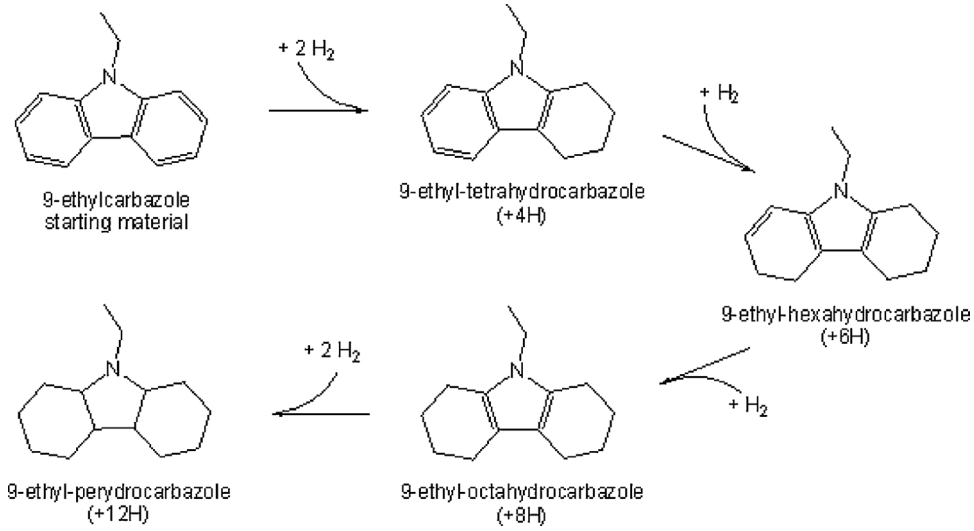

Fig. 5. A simplified scheme containing intermediates and products of catalytic stepwise hydrogenation of 9-ethylcarbazole (+4*H* and +8*H* correspond to four and eight hydrogen atoms added to the starting material, respectively). The +6*H* intermediate was detected only by mass spectrometry (MS), all of the other compounds were detected by both MS and NMR [14].

explained by the fact that the N—H bond is weaker than the C—H bond it replaced [4]. In addition, C—H bonds which are adjacent to an N atom are also weakened as compared to C—H bond in a pure carbocycle, which additionally facilitates the kinetics of hydrogen removal from LOC [4,10,33,34]. For example, Sotoodeh et al. reported dehydrogenation of 9-ethyl-perhydrocarbazole over a silica supported Pd catalyst at 1 bar of He, at 150–170 °C. The reaction followed first-order kinetics with an apparent activation energy of 126.7 kJ/mol and proceeded to 100% conversion and a maximum 69% recovery of the stored H_2 at 170 °C. In comparison, the dehydrogenation of carbazole under the same reaction conditions was found to be more sluggish and only 52.6% of conversion was obtained with 28% of stored hydrogen recovered [32]. As a result, the difference in dehydrogenation kinetics between perhydrocarbazole and 9-ethyl-perhydrocarbazole was attributed to the stronger adsorption of the reaction product (carbazole) of the former on the catalyst surface. In addition, from the dehydrogenation point of view, the *N*-heteroatom polycyclic compounds containing pyridine-like aromatic sextet were found to have significantly lower standard enthalpy of hydrogenation as compared to their carbocyclic counterparts [34]. Therefore, it could be expected that polycyclic catalytic pairs such as acridine-perhydroacridine would have fast kinetics of hydrogen release. Nevertheless, studies dealing with catalytic dehydrogenation of perhydroacridine are rather scarce in the open literature and the process was reported to be challenging [35]. Only very recently the dehydrogenation of

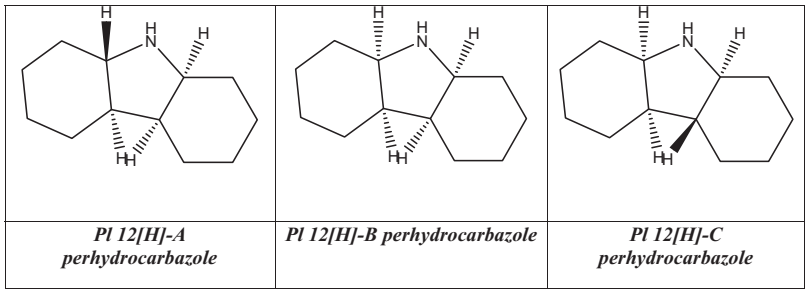

Fig. 6. Three stereoisomers of a fully hydrogenated carbazole.

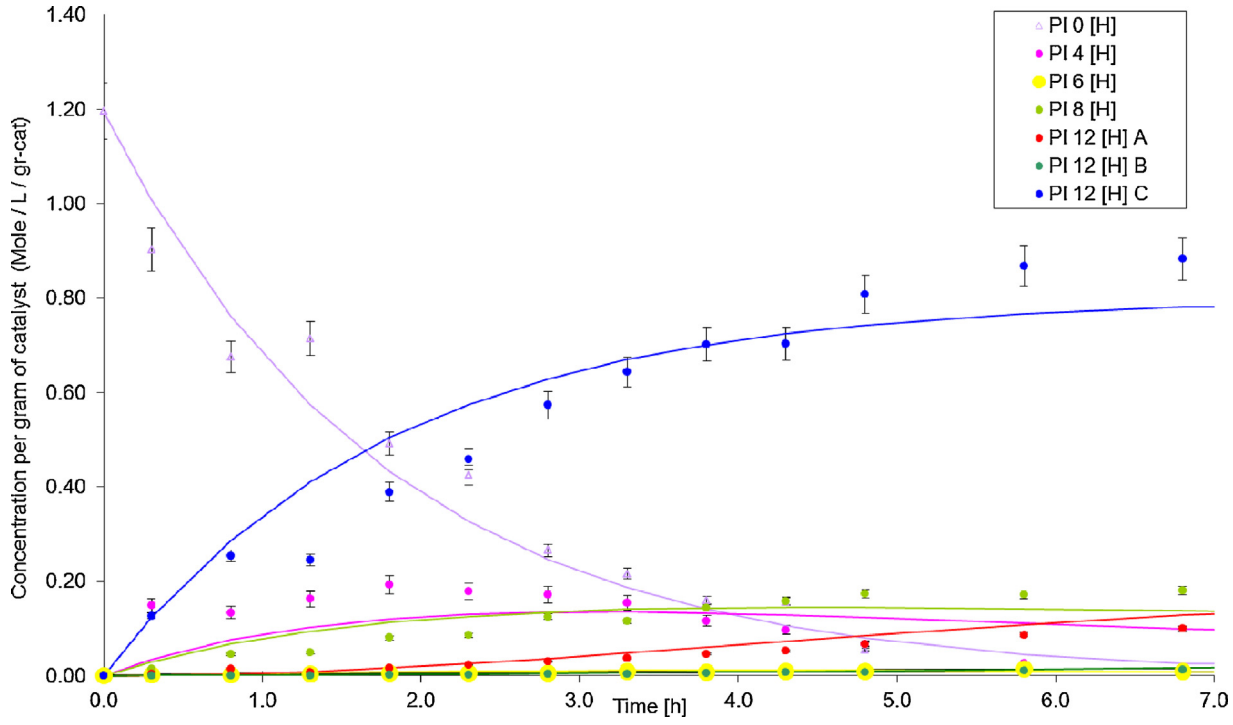

Fig. 7. Time dependent product distribution in carbazole hydrogenation over ruthenium black catalyst. The acronyms of the intermediates as explained in the text.

perhydroacridine was reported using cyclometalated iridium complexes and 97% yield of acridine was obtained under reflux in 20 h, which is too long time for commercial application of this process [36].

3.3. *Influence of the structure of LOH on its ability to hydrogenate*

In the present work, the hydrogenation of various LOCs (showed in Table 1) was explored over Ru black catalyst regarding the influence of the compounds structure on the hydrogen loading step.

3.3.1. *Influence of the length and composition of the side chain*

In order to study the influence of the side chain on the molecules ability to be hydrogenated, the following compounds were considered: 9-ethylcarbazole, carbazole and 9*H*-carbazole-9-ethanol, which are showed in Fig. 4 below.

We have previously reported the catalytic hydrogenation of 9-ethylcarbazole (ETH) over Ru black catalyst and found the stepwise hydrogenation intermediates shown in Fig. 5 [14,15].

Similarly, in hydrogenation of carbazole (CAR) over Ru black, the following intermediates and products were found: tetrahydrocarbazole (Pl 4[H]), hexahydrocarbazole (Pl 6[H]), octahydrocarbazole (Pl 8[H]) and three stereoisomers of the fully hydrogenated perhydrocarbazole (Pl 12[H] A, Pl 12[H] B and Pl 12[H] C). The structures of the three stereoisomers of perhydrocarbazole are showed in Fig. 6.

Comparable intermediates and products were previously observed in the hydrogenation of carbazole over supported ruthenium [37] and calculated on molybdenum catalyst [38]. In addition, these corresponded well with the intermediates and products identified in hydrogenation of 9-ethylcarbazole (ETH) substrate over the same catalyst [15,16].

It is interesting to note from the time dependent product distribution shown in Fig. 7 suggests that the octahydrocarbazole, (Pl 8[H] in CAR hydrogenation) is one of the main intermediates, which is similar to the Pl 8[H] in the ETH hydrogenation. However, this octahydrocarbazole intermediate is considerably less stable as compared to the 9-ethyl-octahydrocarbazole (Pl 8[H] in ETH hydrogenation) intermediate in case of the hydrogenation of the ETH substrate [14].

In comparison, after extended time of the hydrogenation of CAR (20 h), only 4% of Pl 8[H] was detected in the final reaction mixture, whereas in the hydrogenation of ETH, there was no significant decrease in the amount of Pl 8[H] intermediate even after 30 h of reaction and its concentration remained at 40% selectivity [14]. Taking the concentration versus time profile obtained in carbazole hydrogenation showed in Fig. 7 as a starting point, a kinetic model shown in Fig. 8 was established for this reaction. The reaction rates for the formation of each of the intermediates are summarized in Table 3. It is particularly noted that a very good agreement was achieved between the values predicted by the model and those obtained experimentally, which is showed by the considerably close fit of the modelled data (lines) and experimental results (points) in Fig. 7 In order to display more clearly the relevance of the proposed kinetic model, the enlarged part of Fig. 7 containing the products and intermediates which appeared at low concentration is included in Supplementary material, Fig. 1s.

In accordance with this kinetic model and the derived rate constants, the following pathways of hydrogenation of carbazole can take place: there is a direct pathway, possibly via a strong

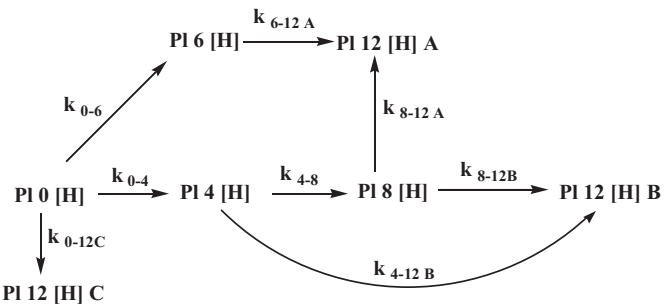

Fig. 8. A kinetic model of carbazole hydrogenation over ruthenium black catalyst with numbered rate constants of the intermediate reactions.

Table 3
The rate constants for each of the intermediates and products in hydrogenation of carbazole.

k_{0-12C} (h^{-1})	k_{8-12B} (h^{-1})	k_{0-4} (h^{-1})	k_{4-8} (h^{-1})	k_{6-12A} (h^{-1})	k_{0-6} (h^{-1})	k_{8-12A} (h^{-1})	k_{4-12B} (h^{-1})
0.30	0.029	0.20	0.30	0.03	0.07	0.11	0.89

adsorption on terrace sites of the catalyst, resulting in the formation of Pl 12[H] C trans-stereoisomer of perhydrocarbazole. Another parallel route is via the Pl 4[H] intermediate, which leads to the formation of the Pl 12[H] B cis isomer or the Pl 12[H] A isomer via the Pl 8[H] intermediate. Additional possible hydrogenation pathway of carbazole is via Pl 6[H] which can produce the fully hydrogenated Pl 12[H] A. It should be noted from the intrinsic high rate constants that the formation of perhydrocarbazole isomer B (Pl 12[H] B) is dominant over other products of this reaction. This isomer is the cis-stereoisomer (based on the GC–MS analysis) that is most desirable from the point of view of the application of this material in hydrogen storage, as it was previously mentioned. It should be noted that CAR possesses the shortest side chain consisting of only one single hydrogen atom. This compound also has the lowest molecular mass and thus the highest theoretical hydrogen carrying capacity from all of the three heterocyclic structures studied here. Additionally, the nitrogen atom in CAR gives the weakest basicity due to lack of induction effect from alkyl group. These types of compounds are generally known to be more difficult to hydrogenate than their basic counterparts [38]. Moreover, the delocalization of the lone pair of electrons from nitrogen in the aromatic ring network renders the adsorption of CAR molecule lying parallel on Ru metal surface [12]. However, once the aromaticity is broken by the partial hydrogenation of at least one double bond in one of the aromatic rings of carbazole, the lone pair of electrons becomes more localized on the nitrogen atom, making it more available for binding to the metal surface for further stepwise hydrogenation [39]. In contrast, the alkyl side chain bonded directly to the N heteroatom in ETH substrate prohibits perpendicular adsorption of 9-octahydro-ethylcarbazole, providing a steric hindrance effect which blocks strong adsorption. This may explain the lower kinetic stability of the octahydrocarbazole intermediate in the case of CAR hydrogenation as opposed to the 9-ethyl-octahydrocarbazole in ETH hydrogenation.

In order to appreciate the thermodynamics in the formation of intermediates and products in CAR hydrogenation over Ru black catalyst, quantum mechanics DFT calculations were performed to evaluate their energetics. In these calculations the sum of electronic energies derived from geometry, thermal, translational and vibrational energies of the intermediate ($C_{12}H_{9+2n}N$) was compared to the sum of enthalpies of the substrate ($C_{12}H_9N$) and enthalpies of the moles of hydrogen used to produce the particular intermediate (nH_2). The results of DFT calculations in case of carbazole hydrogenation are showed in Fig. 9. For comparison, the corresponding results of similar calculations for products and intermediates 9-ethylcarcazole hydrogenation is showed in Fig. 10. The values reported in these figures are consistent with the differences of enthalpies of dissociation of possible configurations of products and intermediates in the hydrogenation at a finite temperature of 130 °C and at atmospheric pressure. These enthalpies were derived using the equations showed in Figs. 9 and 10. In case of products and intermediates of carbazole hydrogenation, a total of 89 different products and intermediates were modeled (Fig. 9). These results were compared to the trends obtained using the same method for 9-ethylcarbazole hydrogenation (Fig. 10) [14]. From this comparison, it can be noticed that the enthalpies of corresponding intermediates and products are lower in case of carbazole (CAR) than 9-ethylcarbazole (ETH) suggesting that the former is easier to hydrogenate with higher conversion than the latter, which is in agreement with experimental results (Table 5, further in the text).

It should be noted that the more negative the enthalpy values, the more stable the intermediate species are. Theoretically, for a number of atom arrangements, some forms of Pl 4[H], Pl 6[H], Pl 8[H], Pl 10[H] and Pl 12[H] appear to be more energetically favorable than the reactants in case of both hydrogenation reactions. In general, the calculations agreed well with the intermediates and products observed during the two hydrogenation reactions. There is in fact an energy penalty observed in both 9-ethyl-dihydrocarbazole and dihydrocarbazole (Pl 2[H]) and thus none of such intermediate was found in neither of the reaction mixtures. In addition, in the hydrogenation of CAR, the difference between the enthalpy of Pl 8[H] intermediate and the fully hydrogenated Pl 12[H] is much larger (169.83 kJ/mol), than ETH (53 kJ/mol). This suggests that in case of CAR, it is more energetically favored to convert Pl 8[H] into fully saturated Pl 12[H] as opposed to the case of ETH. This finding also agrees well with our

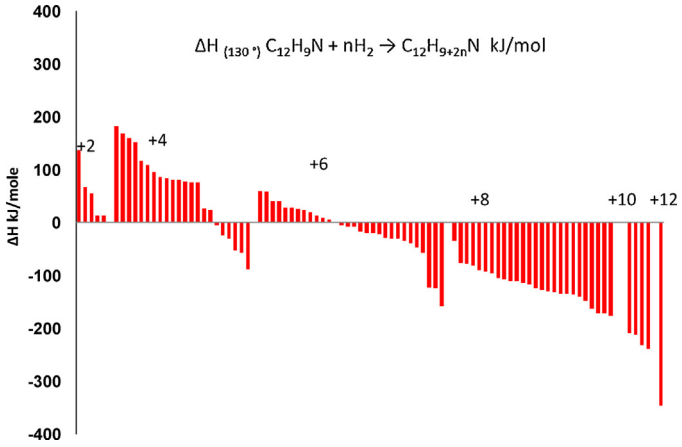

Fig. 9. DFT calculated enthalpy difference (*y*-axis) between carbazole substrate and various hydrogenation intermediates (moles of hydrogen added to create the defined intermediate products in *x*-axis) in a gas phase.

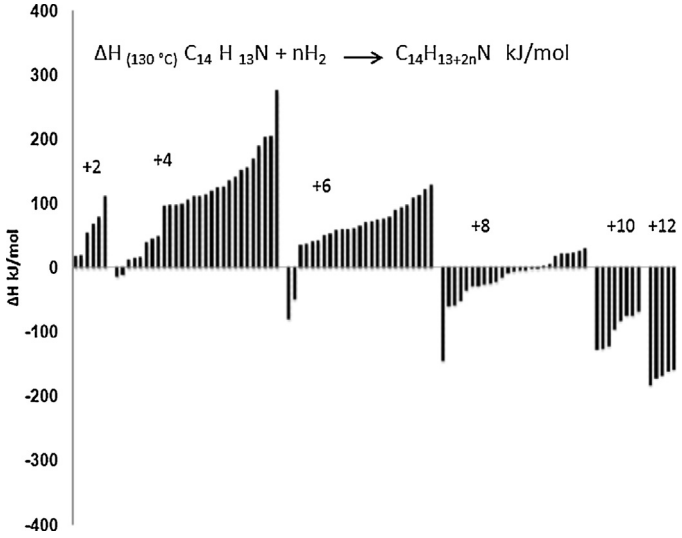

Fig. 10. DFT calculated enthalpy difference (*y*-axis) between 9-ethylcarbazole substrate and various hydrogenation intermediates (moles of hydrogen added to create the defined intermediate products in *x*-axis) in gas phase adapted from [14].

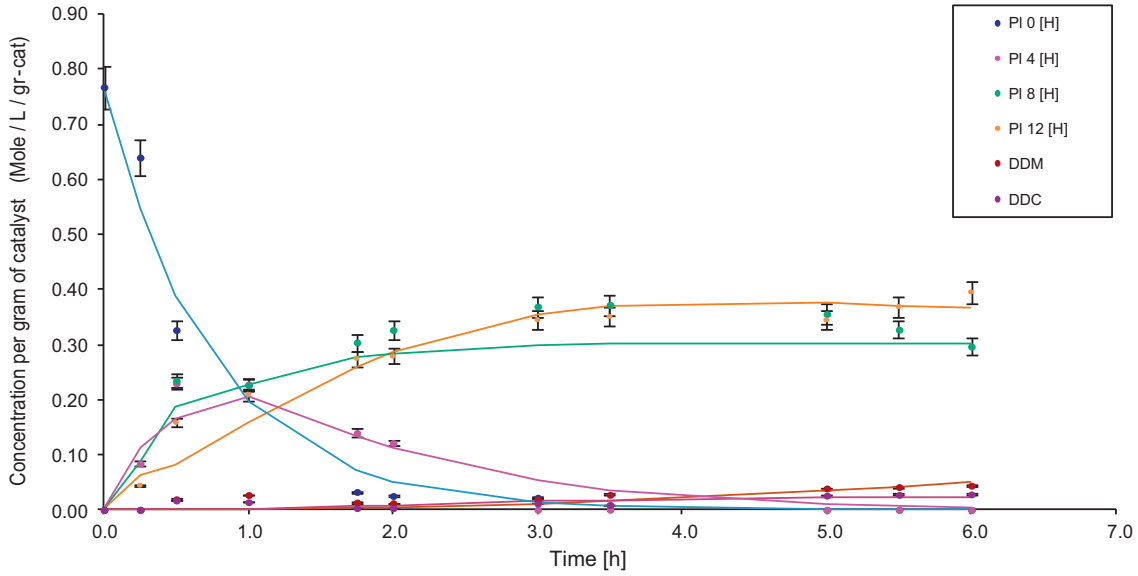

Fig. 11. Product distribution versus time for hydrogenation of 9*H*-carbazole-9-ethanol (HCE) over ruthenium black catalyst.

experimental results. However, there are also clear discrepancies between DFT calculations and our experimental results. For example, the theoretical calculations for both of the reactions suggest that some Pl 10[H] intermediates could be formed in these reactions, but they were not observed in neither of them. Moreover, DFT calculations give only one the most stable stereoisomer of perhydrocarbazole (Pl 12[H]) whereas GC–MS analysis showed three different stereoisomers of this product (see Fig. 6). These differences suggest that kinetic barriers for some elementary reactions are playing key roles in the resulting intermediates and product selectivity of these stepwise hydrogenation reactions.

With regards to the influence of the length of the side chain on the ability of the compound to hydrogenate, the hydrogenation of 9-*H*-carbazole-9 ethanol (HCE) was conducted over the same catalyst and under the same reaction conditions. HCE has a lower melting point than CAR (78 °C versus 246 °C) but slightly higher than that of ETH (68 °C). This may allow the hydrogenation of HCE in a molten state without the use of solvent, which would maximize the practical hydrogen carrying capacity. Unfortunately, the presence of bulky side chain decreases the theoretical hydrogen uptake capacity to 5.4 wt% as compared to that of carbazole (6.7 wt%) or 9-ethylcarbazole (5.8 wt%).

The identified products of hydrogenation of HCE using GC–MS suggest similar consecutive addition of hydrogen atoms to the double bonds in the aromatic rings. The following products were identified by GS–MS in the reaction solution: 9-*H*-tetrahydrocarbazole-9-ethanol (Pl 4[H]), 9-*H*-hexahydrocarbazole-9-ethanol (Pl 6[H]) 9-*H*-octahydrocarbazole-9-ethanol (Pl 8[H]) and one isomer of the fully hydrogenated 9-*H*-perhydrocarbazole-9-ethanol (Pl 12[H]). Based on the observed time-concentration profiles for substrate, intermediates and products (the *y*-axis in Fig. 11 is expressed as concentration per unit mass of catalyst, thus reactivity of a substrate per unit mass of catalyst as well as the substrate reactivity for the production of a particular product (intermediate) per mass of catalyst are obtained), a kinetic model for hydrogenation of HCE was developed and it is shown in Fig. 12. The calculated rate constants for each of the intermediate reactions are gathered in Table 4.

In accordance with the time-concentration profiles and the optimized kinetic model (Fig. 12), there are two parallel routes for the hydrogenation reaction of HCE, one is starting from Pl 8[H] intermediate and leads to the formation of Pl 12[H] product via a series of sequential hydrogenations, similarly to hydrogenation of CAR and ETH. It is noted that 9-octahydrocarbazole-9-ethanol (Pl [8]) intermediate has a similar structure to the structure of 9-ethyl-octahydrocarbazole and octahydrocarbazole. It can be concluded that the high kinetic stability of pyrrolic ring renders the presence of Pl 8[H]s in reaction solutions in case of these three substrates. Due to the longer side chain offering the steric effect, the Pl 8[H] re-adsorption and further hydrogenation on the surface of ruthenium black catalyst is severely hindered. As a result, the rate constant of conversion of Pl 8[H] to Pl 12[H] in hydrogenation of HCE is much lower than that of its formation (see Table 4). The alternative hydrogenation pathway of HCE is via the formation of the Pl 4[H] intermediate. As seen in Fig. 11, the Pl 4[H] intermediate is rapidly converted into the final product and the rate constant of this reaction is one order of magnitude higher than the rate constant of production of Pl 12[H] from Pl 8[H]. Apart from the typical products of the consecutive hydrogenation reactions, two other compounds namely; 9-*H*-dodecahydro-carbazole (DDC) and 9-*H*-dodecahydro-methyl-carbazole (DDM) were additionally identified in this reaction by GC analysis.

These compounds appear to be the products of stepwise hydrogenolysis of the side chain connected to nitrogen in 9*H*-perhydro-carbazole-9-ethanol (Pl 12[H]). Interestingly, such hydrogenolysis of the side chain takes place only after the complete saturation of the aromatic rings. The terminal —OH group plays a crucial role in enhancing the adsorption of the side chain of the molecule on the surface of the catalyst and thus increases the hydrogenolysis reactivity [40]. In this reaction, the rupture of C—C and C—N bonds takes place. The dissociation energies of C—C and

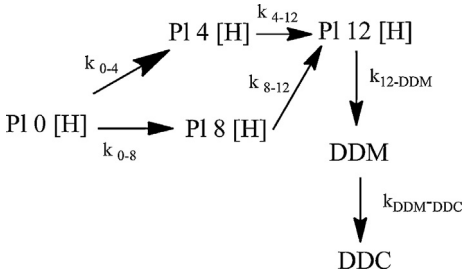

Fig. 12. Reaction model of HCE hydrogenation over ruthenium black; DDM—9-*H*-dodecahydro-methyl-carbazole and DDC-9-*H*-dodecahydro-carbazole.

Table 4
First order rate constants for hydrogenation of HCE over ruthenium black catalyst.

k_0 (h^{-1})	k_{0-4} (h^{-1})	k_{0-8} (h^{-1})	k_{8-12} (h^{-1})	k_{4-12} (h^{-1})	k_{12-DDM} (h^{-1})	$k_{DDM-DDC}$ (h^{-1})
1.30	0.78	0.54	0.10	1.02	0.04	0.62

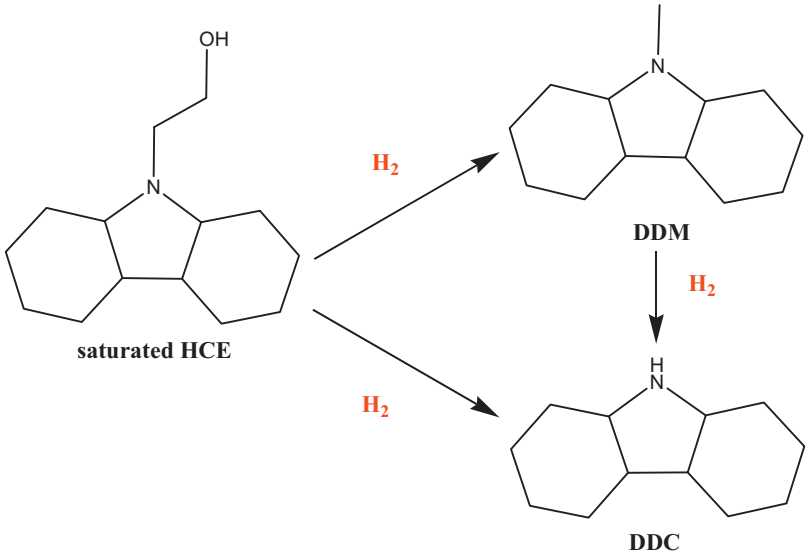

Fig. 13. Possible pathways of hydrogenolysis of the side chain of the fully saturated 9*H*-carbazole-9-ethanol (HCE) over ruthenium black catalyst. The acronyms are explained in the text.

C—N are almost identical (±80 kcal/mol) [41], therefore the order in which the bonds rupture is probably dictated by the steric effects. However, it is not clear from the experimental results obtained whether these reactions take place simultaneously/competitively or as consecutive/stepwise reactions (see Fig. 13 for pathways of hydrogenolysis). However, in our model (Fig. 12), only when a step-wise hydrogenolysis from Pl 12[H] to DDC or to DDM was considered, significant rate constants were obtained in the calculations. Overall, the experimental results showed good agreement with the theoretical model (see Fig. 11). In order to display more clearly the relevance of the proposed kinetic model, the enlarged part of Fig. 11 containing the products and intermediates which appeared at low concentration is included in Supplementary material, Fig. 2s.

To obtain the influence of the side chain on the catalytic hydrogenation reaction, the resulting conversion and selectivity at the initial stage of the reaction (2 h) and at the extended reaction time (20 h) were also compared in order of increasing length of a side chain; from carbazole to 9-ethylcarbazole and 9-*H*-carbazole-ethanol. The results are gathered in Table 5. As summarized in this table, lower conversion in 2 h reaction time (45% versus 59%) was achieved ETH with ethyl chain as compared to CAR with only hydrogen as a side chain. This result can be primary attributed to the thermodynamic factors. Additionally, lower activity of ETH in hydrogenation agrees well with the reports in the literature describing considerably decreased reactivity of carbazoles with alkyl substitution adjacent to the heteroatom as compared to the unsubstituted carbazole [42,43]. Additionally, it is noted that Pl 8[H] intermediate is formed at significantly higher quantity in the hydrogenation of ETH than in hydrogenation of CAR at the complete conversion, which can be attributed to the steric effect of the side chain as discussed before.

In contrast to these results, the presence of —OH group in case of HCE facilitates adsorption of the substrate and intermediates, giving an apparent higher conversion as compared to CAR and ETH. It is thus clear that the substituent —OH group or other moiety groups with strong metal affinity (with lone pairs) can act as another adsorption site on surface of the metal. A similar effect was observed in carbethoxypyrroles [43]. On the other hand, it is also noted that hydrogenolysis of the —OH side chain can take place. Overall, the results show clearly that the thermodynamic and steric effects introduced by the side-chain can have significant influence on the reaction rate and selectivity.

3.3.2. *Substitution of pyrrole with corresponding pyridinic ring*

In order to elute the influence of the substitution of five-membered pyrrole ring with six-membered pyridinic ring, the hydrogenation of acridine was studied. The comparison of carbazole and acridine structures in showed in Fig. 14.

The main products detected by GC–MS in the hydrogenation of acridine over ruthenium black catalysts were: Pl 2[H]-dihydroacridine, Pl 4[H]-tetrahydroacridine, Pl 8[H]-octahydroacridine, and three stereoisomers of the fully hydrogenated Pl 12[H]-perhydroacridine. As it can be seen from Fig. 15, in the hydrogenation of acridine, the main intermediate observed was also octahydroacridine (Pl 8[H]) with two benzenoid rings hydrogenated. Nevertheless, the products and intermediates of this reaction appeared to be more complex as a result of additional reaction steps and intermediates as compared to that of carbazole hydrogenation. Notably, the concentration of Pl 2[H] was much higher and appeared to be more stable as further hydrogenation

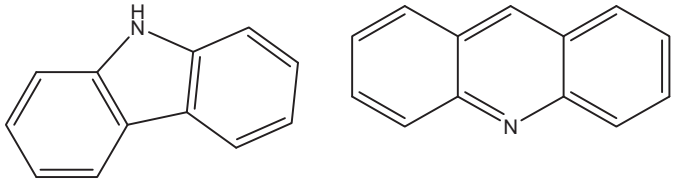

Fig. 14. Comparison of the structures of acridine and carbazole.

Table 5
Comparison of the results of liquid phase hydrogenation of heterocyclic compounds with various lengths and compositions of the side-substituents. The selectivity toward Pl 12[H] is the sum of selectivities toward Pl 12 [H] isomers—where applicable.

Molecule	Time (h)	Conversion (%)	Selectivity (%)				
			Pl 4[H]	Pl 6[H]	Pl 8[H]	Pl 12[H]	Other
CAR	2	59	31	0	12	57	–
	20	100	0	1	4	95	–
ETH	2	45	83	Trace	8	9	–
	20	100	2	Trace	44	54	–
HCE	2	97	16	1	43	38	2
	20	100	0	1	5	34	60

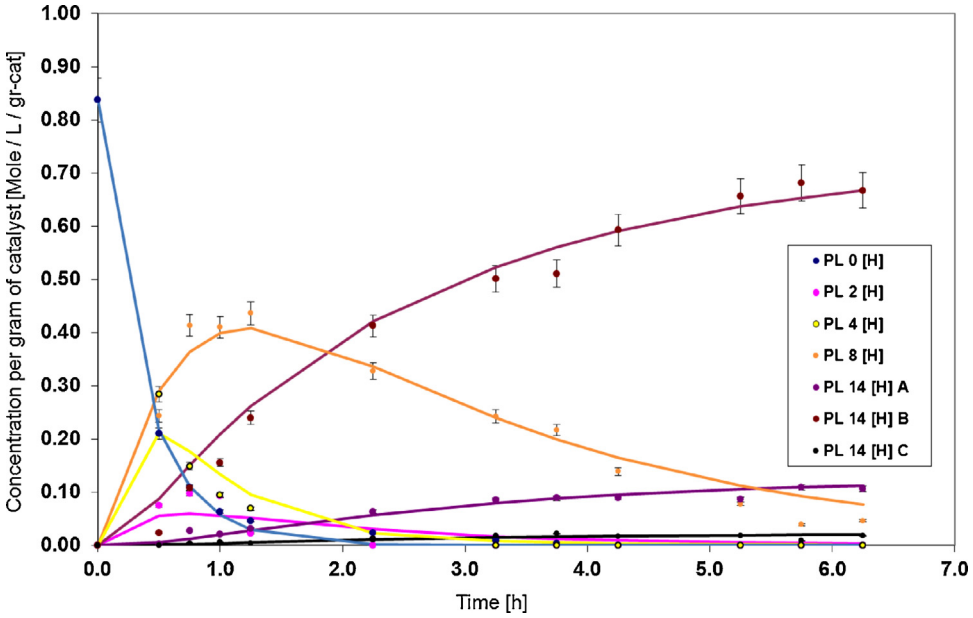

Fig. 15. Product distribution over time for hydrogenation of acridine over ruthenium black catalyst.

proceeded over Ru black catalyst. This observation is in agreement with the literature findings, where the formation of dihydroacridine was reported over NiMo/Al_2O_3 catalyst [44], Raney nickel [42] and supported Pd and Pt catalysts [11,45]. In contrast, the hydrogenation of carbazole with pyrrole ring, did not involve formation of dihydro (Pl 2[H]) intermediate over Ru black.

A reaction model based on product analysis was established as showed in Fig. 16 and the rate constants were derived accordingly and are gathered in Table 6. Notice that this first order reaction model for the acridine hydrogenation over ruthenium black catalyst fitted very well with the experimental data (Fig. 15). Nevertheless, in order to display more clearly the relevance of the proposed kinetic model, the enlarged part of Fig. 15 containing the products and intermediates which appeared at low concentration is included in Supplementary material, Fig. 3s. Comparing the rate constants of carbazole hydrogenation, the rate constant of Pl 8[H] formation was two times higher than that of its further

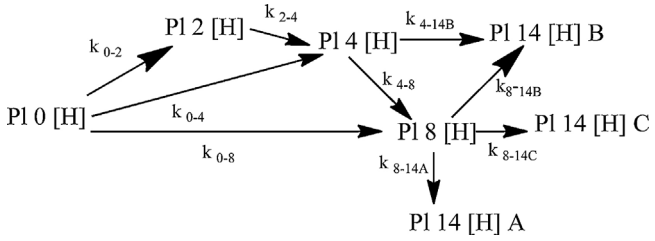

Fig. 16. Reaction model for hydrogenation of acridine over ruthenium black catalyst.

hydrogenation (see Table 3), whereas in case of acridine, the rate constant of Pl 8[H] production was more than five times higher than that of its disappearance (Table 6). It is believed that further conversion of Pl 8[H] similarly to what was observed in case of hydrogenation of CAR, depends on the adsorption through the nitrogen atom which is significantly hindered in octahydroacridine by the presence of the two bulky rings. The presence of these partially saturated rings makes the readsorption of Pl 8[H] intermediate on the catalyst surface difficult to take place.

This finding corresponds well with the steric hindrance created by the ethyl side chain of N atom in 9-ethyl-octahydrocarbazole (Pl 8[H]), which was observed in our previous work [14]. In addition, it is noted that the basicity of acridine is higher than that of the other compounds studied here, since the lone pair of electrons is localized on the nitrogen and therefore a higher degree of adsorption over metal catalyst is expected to take place [46]. In fact, the hydrogenation of acridine progressed very rapidly as compared to that of the other compounds reported here and around 90% of conversion of the substrate was obtained within 30 min of reaction. The fast rate of acridine hydrogenation was also reported in the literature [11,35,45]. As a result, the rate constants derived from our model (Table 6) are considerably higher than corresponding rate constants in the CAR hydrogenation (Table 3).

It was previously reported by Sun et al. [43] that the energy levels of LUMO and HOMO for basic heterocyclic compounds are lower than those for corresponding non-basic compounds. Therefore, the transfer of electrons from basic substrate to metal catalyst surface is energetically more favourable. Ruthenium is a typical electron deficient metal, therefore it is logical that it is more likely to accept

Table 6
Calculated rate constants of hydrogenation of acridine over ruthenium black catalyst.

k_0 (h^{-1})	k_{0-2} (h^{-1})	k_{0-4} (h^{-1})	k_{2-4} (h^{-1})	k_{4-8} (h^{-1})	k_{0-8} (h^{-1})	k_{8-14B} (h^{-1})	k_{8-14A} (h^{-1})	k_{8-14C} (h^{-1})	k_{4-14B} (h^{-1})
2.90	0.29	1.70	0.60	1.50	0.88	0.32	0.08	0.01	0.75

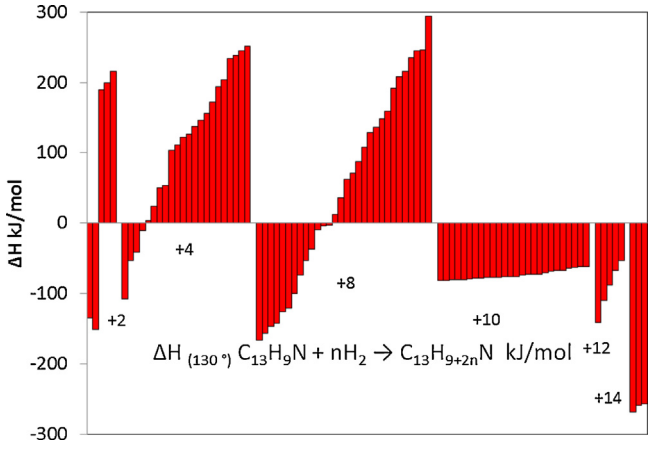

Fig. 17. DFT calculated enthalpy difference (*y*-axis) between acridine substrate and its hydrogenation intermediates (moles of hydrogen added to create the defined intermediate products in *x*-axis) in the gas phase approximation.

electrons and as a result basic compounds (electron donors such as acridine) show higher adsorption strength and higher reaction rates over this catalyst.

Fig. 17 shows the differences in values of enthalpies of dissociation of products and intermediates in case of hydrogenation of acridine obtained by DFT calculations using the equation showed on the aforementioned figure. The DFT method used for these calculations was the same as the one used to obtain the results for carbazole hydrogenation (Fig. 9) and 9-ethylcarbazole hydrogenation (Fig. 10).

The calculations also agreed well with the experimental results. It is interesting to note that the calculated enthalpy for the Pl 2[H] is almost as low as for Pl 8[H] showing that these two intermediates are very likely to be produced in the hydrogenation of acridine, as indeed observed experimentally in the product mixtures. The partial hydrogenation to Pl 2[H] in this pyridine ring will not cause the electrons delocalization in this structure. On the contrary as shown earlier in this work, there is a large energy penalty to hydrogenate carbazole to dihydrocarbazole (Pl 2[H]) due to a clear break of aromatization (delocalization of electrons). As a result, Pl 2[H] intermediate was not observed in hydrogenation of CAR. On the other hand, although Pl 10[H] and Pl 12[H] are thermodynamically favorable in hydrogenation of acridine, they were not observed in our reaction mixtures. It is believed that the stronger adsorption through the N atom can take place in the solution, which allows rapid conversion of these intermediates to the fully saturated products. Particularly, the cyclic alkene intermediate (Pl 12[H]) with only one remaining unsaturated double bond is very unstable in the solution and therefore will be quickly hydrogenated further to the fully saturated products, perhydroacridine (Pl 14[H]). Also, such hydrogenation of remaining single double bond is known to imply low energy barrier in case of naphthalene hydrogenation [46]. Thus, none of these intermediates were observed in the analyzed reaction solutions. These findings agree well with the results of hydrogenation of acridine over Pt, Rh and Pd [11]. In addition, we have observed three stereoisomers of acridine in the above experiment, similar to those previously reported [47]. The calculated three different stereoisomers of the fully saturated perhydroacridine (see Fig. 17) also agreed well with the experimental observations.

4. Conclusion

As shown from our results, the structure of LOC molecule can clearly affect the elementary hydrogenation step(s) on metal catalyst surface. This implies that a careful design of heterocycle structure for improved hydrogen uptake value with favourable thermodynamics and fast kinetics is very important. The biggest challenge is that the unsaturated structure has to favour hydrogen release or uptake steps reversibly and readily under chosen reaction conditions without compromising poor thermodynamics and kinetics of these reactions. Both directions of the process have to be viable, implying moderate endothermicity of the dehydrogenation step. Thus, in order to select the best candidate for LOC the key physical parameter that should be accounted for is the enthalpy of hydrogenation/dehydrogenation of these compounds. From the point of view of fuel recovery step, acridine seems to be the best candidate amongst the four related compounds studied, due to the favourable fast kinetics and thermodynamics of hydrogenation and at the same time, high hydrogen uptake capacity of 7.2 wt%. However, the dehydrogenation of acridine has been reported in the literature to be a difficult process, resulting in poor yields despite the use of high catalyst content and elevated temperatures [35] or long reaction times [36]. In addition, the hydrogenation of acridine appears to produce a range of intermediates which are more complex than those of CAR and ETH over the same catalyst. In the case of CAR molecule, further introduction of alkyl substituent groups, although can lower the melting point of nitrogen heterocycles, it also decreases the theoretical hydrogen uptake capacity of the material. In addition, alkyl side chains can introduce steric hindrance effect depending on their structures that could lead to formation of kinetically stable intermediates. For example, incorporation of hydroxyl group although can increase the hydrogenation reactivity of the LOC, such group is susceptible to hydrogenolysis, which decreases the overall recyclability of the carrier, as demonstrated in the present work. On the contrary, the dehydrogenation of 9-ethyl-perhydrocarbazole was reported to be more facile than the dehydrogenation of perhydrocarbazole under the same reaction conditions, due to the presence of the ethyl side chain in the former [12].

Regarding the size of the heterocyclic ring in the LOH, clearly five member rings should be more preferred over six member rings. This is with agreement to the findings considering dehydrogenation of similar heterocyclic systems, where moving from six membered to five membered rings with incorporated N-atom lowered the dehydrogenation temperature [10]. Moreover, it is known that the substitution of hydrogen with side groups can improve the physical properties of the hydrogen carrier from the point of view of dehydrogenation step. Nevertheless, as it is evident from our results, the use of *N*-heterocyclic compounds with polar alkyl side chains containing atoms with lone pair electrons (i.e. oxygen) is not suitable for the application in hydrogen storage. Further studies will be focused on the influence of the type of heteroatom on the hydrogenation activity of five-membered structures.

Acknowledgments

Dr K. Tam from Astra Zeneca, Dr K. M. Kerry Yu, Mr Fernando Eblagon, Dr Anibal J. Ramirez-Cuesta are acknowledged for fruitful discussions and help in data analysis. The authors are indebted to

the University of Oxford, EPSRC and ISIS, UK for financial support of this project.

Appendix A. Supplementary data

Supplementary material related to this article can be found, in the online version, at http://dx.doi.org/10.1016/j.apcatb.2014.04.044.

References

[1] S. Yolcular, O. Olgun, Catal. Today 13 (2008) 198–202.
[2] Y. Okada, E. Sasaki, E. Watanabe, S. Hyodo, H. Nishijima, Int. J. Hydrogen Energy 31 (2006) 1348–1356.
[3] R.B. Biniwale, S. Rayalu, S. Devotta, M. Ichikawa, Int. J. Hydrogen Energy 33 (2008) 360–365.
[4] R. Crabtree, Energy Environ. Sci. 1 (2008) 134–138.
[5] F. Alhumaidan, D. Cresswell, A. Garforth, Energy Fuels 25 (2011) 4217–4234.
[6] N. Hiyoshi, R. Miura, C.V. Rode, O. Sato, M. Shirai, Chem. Lett. 34 (2005) 424–425.
[7] D. Teichmann, W. Arlt, P. Wasserscheid, R. Freymann, Energy Environ. Sci. 4 (2011) 2767–2773.
[8] D.E. Schwarz, T.M. Cameron, P.J. Hay, B.L. Scott, W. Tumas, D.L. Thorn, Chem. Commun. (2005) 5919–5921.
[9] A. Shukla, S. Karmakar, R.B. Biniwale, Int. J. Hydrogen Energy 37 (2012) 3719–3726.
[10] E. Clot, O. Eisenstein, R.H. Crabtree, Chem. Commun. (2007) 2231–2233.
[11] K. Sakanishi, M. Ohira, I. Mochida, H. Okazaki, M. Soeda, Bull. Chem. Soc. Jpn. 62 (1989) 3994–4001.
[12] F. Sotoodeh, K.J. Smith, Ind. Eng. Chem. 49 (2010) 1018–1026.
[13] A. Kalantar Neyestanaki, P. Maki-Arvela, H. Backman, H. Karhu, T. Salmi, J. Vayrynen, D. Yu Murzin, J. Mol. Catal. A: Chem. 193 (2003) 237–250.
[14] K. Morawa Eblagon, K. Tam, K.M.K. Yu, S.-L. Zhao, X.Q. Gong, H. He, L. Ye, L.-C. Wang, A.J. Ramirez-Cuesta, S.C. Tsang, J. Phys. Chem. C 21 (2010) 9720–9730.
[15] K.M. Eblagon, K. Tam, K.M.K. Yu, S.C.E. Tsang, J. Phys. Chem. C 116 (2012) 7421–7429.
[16] K. Morawa Eblagon, K. Tam, S.C.E. Tsang, Energy Environ. Sci. 5 (2012) 8621–8630.
[17] X.-L. Yang, W.-Q. Zhang, C.-G. Xia, X.-M. Xiong, X.-Y. Mua, B. Hu, Catal. Commun. 11 (2010) 867–870.
[18] T. Ishihara, K. Harada, K. Eguchi, H. Arai, J. Catal. 136 (1992) 161–169.
[19] A. Basinska, J. Stoch, F. Domka, Pol. J. Environ. Stud. 12 (2003) 395–400.
[20] K.J. Johnson, Numerical Methods in Chemistry, Marcel Dekker, New York, NY, 1980.
[21] J.A. Nelder, R. Mead, Comput. J. 7 (1965) 308–313.
[22] C. Huber-Carol, N. Balakrishnan, M. Nikulin, M. Mesbah, Goodness-of-Fit Test and Model Validity, Birkhauser, Boston, MA, 2002.
[23] Gaussian 03, Revision B.05, Gaussian Inc., Wallingford, CT, 2004.
[24] K. Morawa Eblagon, D. Rentsch, O. Friedrichs, A. Remhof, A. Zuettel, A.J. Ramirez-Cuesta, S.C. Tsang, Int. J. Hydrogen Energy 35 (2010) 11609–11621.
[25] J.B. Foresman, A. Frish, Exploring Chemistry with Electronic Structure Methods, second ed., Gaussian Inc., Pittsburgh, PA, 1998.
[26] C.L. Bianchi, M. Cattana, V. Ragaini, Mater. Chem. Phys. 29 (1991) 297–306.
[27] Y.V. Larichev, J. Phys. Chem. C 112 (2008) 14776–14780.
[28] L.A. Pedersen, J.H. Lunsford, J. Catal. 62 (1980) 39–47.
[29] B.M. Faroldi, E.A. Lombardo, L.M. Cornaglia, Appl. Catal., A: Gen. 369 (2009) 15–26.
[30] X. Zhou, T. Wu, B. Hu, T. Jiang, B. Han, J. Mol. Catal. 306 (2009) 143–148.
[31] M. Nagai, T. Masunaga, Fuel 67 (1988) 771–774.
[32] F. Sotoodeh, L. Zhao, K.J. Smith, Appl. Catal., A: Gen. 362 (2009) 155–162.
[33] G.P. Pez, A.R. Scott, A.C. Cooper, H. Cheng, US Pat. 7101530, 2006 (September 5) (and prior patents cited).
[34] G.P. Pez, A.R. Scott, A.C. Cooper, H. Cheng, F.C. Wilhelm, A.H. Abdourazak, US Pat. 7351395, 2008.
[35] R.M. Acheson, G. Acridines, Heterocycles, second ed., Interscience Publishers, London, 1973.
[36] J. Wu, D. Talwar, S. Johnston, M. Yan, J. Xiao, Angew. Chem. Int. Ed. 52 (2013) 6983–6987.
[37] P. Zeuthen, K.G. Knudsen, D.D. Whitehurst, Catal. Today 65 (2001) 307–314.
[38] H. Tominaga, M. Nagai, Appl. Catal., A: Gen. 389 (2010) 195–204.
[39] M.J. Girgis, B.C. Gates, Ind. Eng. Chem. Res. 30 (1991) 2021–2058.
[40] J.L. Rainey, H. Adkins, J. Am. Chem. Soc. 61 (1939) 1104–1110.
[41] M. Nagai, T. Masunaga, Bull. Chem. Soc. Jpn. 62 (1989) 972–974.
[42] H. Adkins, H.L. Coonradt, J. Am. Chem. Soc. 63 (1940) 1563–1570.
[43] M. Sun, A.E. Nelson, J. Adjaye, J. Mol. Catal. A: Chem. 222 (2004) 243–251.
[44] D. Ferdous, A.K. Dalai, J. Adjaye, Energy Fuels 17 (2003) 164–171.
[45] K. Sakanishi, M. Ohira, I. Machida, H. Okazaki, M. Soeda, J. Chem. Soc., Perkin Trans. 2 (1988) 1769–1773.
[46] P.A. Rautanen, M.S. Lylykangas, J.R. Aittamaa, A.O.I. Krause, Ind. Eng. Chem. Res. 41 (2002) 5966–5975.
[47] T.G. Nikolaeva, P.V. Reshetov, A.P. Krivenko, Chem. Heterocycl. Compd. 33 (1997) 755–772.